Flow properties of immiscible blends: Doi-Ohta model with active advection

Jian Feng Gu and Miroslav Grmela*
Ecole Polytechnique de Montreal, Case Postale 6079 succursale Centre-ville, Montreal, Quebec, Canada H3C 3A7
(Received 28 April 2008; published 11 November 2008)

The interface between two immiscible fluids both is influenced (advected) by the imposed flow and influences (perturbs) it. The perturbation then changes the advection. This phenomenon is taken into account in an extended Doi-Ohta model of rheological behavior of immiscible blends. The agreement of the rheological predictions with experimental data is improved.

DOI: 10.1103/PhysRevE.78.056302 PACS number(s): 47.57.Qk, 47.50.Cd, 47.10.Df

I. INTRODUCTION

The macroscopic flow behavior of immiscible blends cannot be described with only classical hydrodynamic fields serving as state variables. This is because the immiscible blends contain an interface that evolves in time on a time scale comparable with the time scale on which the hydrodynamic fields evolve. In order to model flows of immiscible blends we have to therefore, first, choose a way to describe states of the interface (we shall call it an interface morphology) and, second, find equations governing the time evolution of the morphology and the hydrodynamic fields.

As for the the mathematical characterization of the morphology, we follow in this paper Doi and Ohta [1]. Immiscible blends are assumed to be isothermal, incompressible, and spatially homogeneous. The interface is seen as being uniformly distributed throughout the fluid. Its states are characterized by one tensor $\boldsymbol{q}$ and one scalar Q. The latter is the surface area per unit volume and the former is a symmetric traceless tensor characterizing the orientation of the interface. Other important characteristics of the morphology, as for example the curvature and, more generally, the global shape of the interface, are out of the reach of the Doi-Ohta description. Consequently, the strong points of the Doi-Ohta theory are mathematical simplicity, and rheological (rather than morphological) predictions. Below, we shall extend the Doi-Ohta model in order to be able to account for the flow perturbations caused by the presence of the interface. The extension will not, however, provide a more detailed description of the morphology.

For the imposed overall flow the interface is an obstacle that moves and deforms in response to the forces generated in the fluid-interface interactions and also modifies the flow in its neighborhood. If all the details of (i) the shape of the interface, (ii) interface-fluid interactions (boundary conditions), and (iii) rheological properties of both fluids involved are known, then both the modification of the flow and the modification of the advection can be obtained as a solution to the corresponding Stokes problem. Due to the lack of knowledge of all three points (i)–(iii) mentioned above as well as the enormous mathematical (numerical) complexity involved in the process of solving the Stokes problem, we cannot take this microhydrodynamic path. We only recall that the microhydrodynamics investigation implies that the flow in the vicinity of the interface remains unperturbed (and thus the interface follows passively the flow—a passive advection) only if both fluids in the mixture are identical and the interface is completely structureless and does not interact with the bulk fluid. Otherwise, the flow of the fluid surrounding the interface is always perturbed and the advection of the interface is never passive (we shall call it an active advection). Even if the mechanical properties of the interface as well as the bulk fluid-interface interactions are ignored, just the "rheological inhomogeneity" (i.e., the appearance of regions with different viscosities) is sufficient to create flow perturbations and thus a nonpassive (active) advection.

Doi and Ohta assumed in [1] that the interface is advected passively (i.e., its presence does not perturb the the flow around it). A mesoscopic investigation of the advection that takes into account the active role of the interface in its advection but does not enter into all details needed in the complete microhydrodynamic analysis has been introduced in [2]. Our goal in this paper is to replace the passive advection in the Doi-Ohta model by the active advection introduced in a general form in [2].

The paper is organized as follows. In Sec. II we recall the concept of mesoscopic active advection and the Doi-Ohta model. The governing equations of the Doi-Ohta model with active advection are developed in Sec. III. Predictions of the extended model are compared with predictions of other models and with some published experimental data in Sec. IV.

II. ACTIVE ADVECTION

States of isothermal, incompressible, and homogeneous immiscible blends are described in the Doi-Ohta theory by the field of the overall momentum $\boldsymbol{u}(\boldsymbol{r})$ and by the interface morphology characterized by $\boldsymbol{q}$ and Q; $\boldsymbol{r}$ denotes the position vector, $\boldsymbol{q}$ is a symmetric traceless tensor characterizing the orientation of the interface, and Q is the surface area per unit volume. In order to be able to deal with the active role that the interface plays in the advection, we introduced another tensor $\boldsymbol{w}$ that is closely related to the gradient of the perturbed velocity.

The governing equations of the extended Doi-Ohta theory [a coupled set of equations governing the time evolution of $(\boldsymbol{u},\boldsymbol{q},\boldsymbol{Q},\boldsymbol{w})$] will be constructed in this paper by filling the thermodynamic framework [the general equation for the nonequilibrium reversible-irreversible coupling (GENERIC)]

*Corresponding author. miroslav.grmela@polymtl.ca

with the mesoscopic version of the physics involved in the microhydrodynamic formulation of the Stokes problem. The framework itself guarantees the compatibility of the time evolution with mechanics in the inviscid limit and the compatibility with thermodynamics of externally unforced fluids. The process of filling the framework is called *GENERIC constitutive relations*, just as the process of filling the framework of local balance laws (representing the general framework for governing equations of classical hydrodynamics) is called the *constitutive relations*. In order to prepare the construction of the governing equations of the extended theory we shall recall the GENERIC framework [3–10] (in Sec. II A), generic formulation of the active advection developed in [2] (Sec. II B), and the GENERIC formulation of the Doi-Ohta theory [11,12] (Sec. II C).

A. Thermodynamic (GENERIC) framework

The abstract framework for the governing equations of classical hydrodynamics (the balance laws) arises from requiring mass, momentum, and energy conservation. The filling of the framework, i.e., the specification of the fluxes introduced in the balance laws) is called a constitutive relation. In addition to mass, momentum, and energy conservation, solutions to the hydrodynamic equations are also required to agree with the experimental observations constituting the basis of equilibrium thermodynamics (a fluid that is left undisturbed reaches a state at which its behavior is found to be well described by equilibrium thermodynamics). Consequences of this requirement are explored in nonequilibrium thermodynamics. Still another general aspect of hydrodynamics is its mechanical origin. The balance of momentum has also an alternative interpretation as a continuum version of Newton's law. This mechanical aspect is used in classical hydrodynamics only in providing part of the momentum flux with the physical interpretation of the force acting on a surface. A general framework for the mesoscopic time evolution based on the requirements of the conservation of mass, momentum, and energy, and with equal importance also for the requirement of compatibility with thermodynamics and mechanics is called GENERIC. Its main advantage is its applicability for complex fluids, whose states have to be characterized not only by the classical hydrodynamic fields but also with extra fields characterizing the internal structure. If compared with classical hydrodynamics, the GENERIC viewpoint is particularly new and powerful in requiring compatibility with mechanics. Newton's law enters the analysis not only in providing an alternative physical interpretation to the balance of momentum but also in the discussion of the time evolution of the internal structure. Below, we shall recall the GENERIC framework in the special context of isothermal fluids.

Let x denote the state variables. If we limit ourselves to isothermal and incompressible fluids then the time evolution of x, compatible with thermodynamics and mechanics, is governed by [3–10]

$$\dot{x} = L\Phi_x - \frac{\partial \Xi}{\partial \Phi_x}, \tag{1}$$

called in [7,8] GENERIC. By $\dot{x}$ we denote the time derivative of x. The first term on the right-hand side of (1) expresses compatibility with mechanics, the second the compatibility with thermodynamics. The symbols appearing in (1) have the following meanings.

Free energy. $\Phi(x)$, a real-valued function of x, has the physical meaning of the total free energy. By Φ_x we denote the derivative of Φ with respect to x.

Kinematics. The operator L, hereafter called a Poisson bivector, transforms a covector (a gradient of a potential) into a vector. From the physical point of view, L expresses kinematics of the state variables x. In the particular case of classical mechanics of particles [the state variables in this case are $x=(p,q)$, where q are position vectors and p the momenta of the particles], $L=\left(\begin{smallmatrix}0 & 1\\ -1 & 0\end{smallmatrix}\right)$. This is the Poisson bivector transforming in classical mechanics the gradient of energy $E(q,p)$ into a vector field. In the general setting, L is required to satisfy the following properties: $\{A,B\}=\langle A_x, LB_x\rangle$ is a Poisson bracket, i.e., $\{A,B\}=-\{B,A\}$, and satisfies the Jacobi identity $\{A,\{B,C\}\}+\{B,\{C,A\}\}+\{C,\{A,B\}\}=0$; A,B,C are sufficiently regular real-valued functions of x; $\langle,\rangle$ denotes the inner product. The Poisson bracket corresponding to $L=\left(\begin{smallmatrix}0 & 1\\ -1 & 0\end{smallmatrix}\right)$ is thus $\{A,B\}=A_qB_p-B_qA_p$.

Dissipation. $\Xi(\Phi_x)$, called a dissipation potential, is a sufficiently regular real-valued function of Φ_x satisfying the following properties:

$$\Xi(0) = 0,$$

$$\Xi \text{ reaches its minimum at } 0,$$

$$\Xi \text{ is convex in a neighborhood of } 0. \tag{2}$$

Properties of solutions of (1)

The properties required from L,Ξ appearing in (1) imply that solutions to (1) satisfy the following inequality:

$$\frac{d\Phi}{dt} \leqslant 0. \tag{3}$$

The free energy Φ can thus only remain unchanged or decrease during the time evolution. To see that (3) indeed holds, we note that $d\Phi/dt=\langle\Phi_x, L\Phi_x\rangle-\langle\Phi_x, \partial\Xi/\partial\Phi_x\rangle\leqslant 0$. The last inequality follows from $\langle\Phi_x, L\Phi_x\rangle=0$ and from the properties required from the dissipation potential Ξ. The inequality (3) together with the thermodynamic stability requirement (i.e., Φ is a convex function of x) allows us to consider Φ as a Lyapunov function. This then means that solutions to (1) tend, as $t\to\infty$, to states that minimize the free energy (i.e., the states, called equilibrium states, that are solutions of $\Phi_x=0$). Since the first term on the right-hand side of (1) leaves Φ unchanged, we shall also write (1) as

$$\frac{\partial}{\partial t} = \left(\frac{\partial}{\partial t}\right)_{\text{nondiss}} + \left(\frac{\partial}{\partial t}\right)_{\text{diss}}, \tag{4}$$

where

$$\left(\frac{\partial x}{\partial t}\right)_{\text{nondiss}} = L\Phi_x \tag{5}$$

and

$$\left(\frac{\partial x}{\partial t}\right)_{\text{diss}} = -\frac{\partial \Xi}{\partial \Phi_x}. \tag{6}$$

The framework (1) is filled by specifying the state variables x, the potentials Φ, Ξ, and the operator $L(x)$. A specification of x, Φ, Ξ, L is called a GENERIC constitutive relation. Below, we shall recall two examples (in Secs. II B and II C) and in Sec. III we shall develop a third one as the main result of this paper.

B. GENERIC formulation of active advection

In this section we shall gradually develop the time evolution equations introduced in [2].

1. One-component complex fluid

We begin with a one-component incompressible and isothermal complex fluid whose internal structure (morphology) is chosen to be characterized by a conformation tensor $\boldsymbol{c}$ (a 3×3 symmetric and positive definite matrix). We assume that the complex fluid is homogeneous and thus we consider $\boldsymbol{c}$ to be independent of $\boldsymbol{r}$. Depending on what type of complex fluid and internal structure we consider, the conformation tensor $\boldsymbol{c}$ can have many different physical interpretations. Typically, it is seen as a deformation tensor of the internal structure. In Sec. II C we shall interpret it in the context of the Doi-Ohta characterization of the interface.

We proceed to specify the GENERIC constitutive relations.

State variables. The state variable x in this section is thus

$$x = (\boldsymbol{u}(\boldsymbol{r}), \boldsymbol{c}), \tag{7}$$

where $\boldsymbol{u}(\boldsymbol{r})$ is the field of the overall momentum and $\boldsymbol{c}$ is the conformation tensor.

Kinematics. Next, we need the Poisson bracket expressing kinematics of (7) (see [13–15] and Sec. III A):

$$\begin{aligned}\{A,B\}^{(u,c)} = &\int d\boldsymbol{r}\, u_i[\partial_j(A_{u_i})B_{u_j} - \partial_j(B_{u_i})A_{u_j}] \\ &+ \int d\boldsymbol{r}\, c_{kl}(A_{c_{lm}}\partial_k B_{u_m} - B_{c_{lm}}\partial_k A_{u_m}) \\ &+ \int d\boldsymbol{r}\, c_{km}(A_{c_{lm}}\partial_k B_{u_l} - B_{c_{lm}}\partial_k A_{u_l}).\end{aligned} \tag{8}$$

In the above two equations we use the following notation: $i,j=1,2,3$; $\partial_i = \partial/\partial r_i$; repeated indices mean summation; A and B are sufficiently regular real-valued functionals of $(\boldsymbol{u}(\boldsymbol{r}), \boldsymbol{c})$; $A_{u_i} = \delta A/\delta u_i(\boldsymbol{r})$; δ/δ denotes the Volterra functional derivative.

The equations $(\dot{x})_{\text{nondiss}} = L\Phi_x$ corresponding to the bracket (8) are

$$\begin{aligned}\left(\frac{\partial \boldsymbol{u}}{\partial t}\right)_{\text{nondiss}} &= \nabla(\boldsymbol{u}\boldsymbol{v}) - \nabla p - \nabla\cdot\boldsymbol{\sigma}^{(\text{nd})}, \\ \left(\frac{d\boldsymbol{c}}{dt}\right)_{\text{nondiss}} &= \boldsymbol{c}\cdot\nabla\boldsymbol{v} + \nabla\boldsymbol{v}^T\cdot\boldsymbol{c},\end{aligned} \tag{9}$$

where

$$\boldsymbol{\sigma}^{(\text{nd})} = -2\Phi_{\boldsymbol{c}}\cdot\boldsymbol{c}, \tag{10}$$

p is the hydrostatic pressure, $\boldsymbol{v} = \Phi_{\boldsymbol{u}}$ and the superscript T denotes the transpose. The time derivative in the second equation in (9) is the ordinary derivative (not the partial derivative as in the first equation) since $\boldsymbol{c}$ is, according to our assumption, independent of $\boldsymbol{r}$.

Dissipation. We recall that $\Phi_{\boldsymbol{c}} = 0$ at equilibrium. The thermodynamic force driving the internal structure to its equilibrium is thus $\boldsymbol{X} = \Phi_{\boldsymbol{c}}$. If we limit ourselves to states for which $(\Phi_{\boldsymbol{c}})^k$, $k \geqslant 3$, can be neglected, we choose

$$\Xi = \frac{1}{2}\Lambda \text{tr}(\boldsymbol{X}\cdot\boldsymbol{c}\cdot\boldsymbol{X}), \tag{11}$$

where $\Lambda > 0$ is a phenomenological coefficient. The equation $(\dot{x})_{\text{diss}} = -\partial\Xi/\partial\Phi_x$ becomes thus

$$\begin{aligned}\left(\frac{\partial \boldsymbol{u}}{\partial t}\right)_{\text{diss}} &= 0, \\ \left(\frac{d\boldsymbol{c}}{dt}\right)_{\text{diss}} &= -\frac{1}{2}\Lambda(\boldsymbol{c}\cdot\Phi_{\boldsymbol{c}} + \Phi_{\boldsymbol{c}}\cdot\boldsymbol{c}).\end{aligned} \tag{12}$$

The individual nature of the complex fluid under consideration is expressed in the free energy Φ and the dissipation potential Ξ. In this paper the complex fluid under investigation is an immiscible blend. We shall discuss Φ and Ξ in Sec. III after completing the presentation of the advection.

2. Active advection

As we have already explained in the Introduction, the advection is formulated in the context of microhydrodynamics as the Stokes problem. The existence of a nontrivial solution to the Stokes problem implies that the advection is not passive (i.e., it is active in our terminology). How can we discuss active advection on a mesoscopic level on which we cannot formulate the Stokes problem? We shall follow here the approach developed in [2]. In this section we shall recall the mathematical formulation. The physics behind it is discussed in Sec. III A.

In order to be able to account for changes in the imposed flow caused by the flow-interface interaction, we introduce a new state variable $\boldsymbol{w}$ that is a 3×3 tensor whose relation to the perturbed flow will become clear later [see Eq. (14) and also Sec. III A] when its role in the time evolution is revealed.

State variables

$$x = (\boldsymbol{u}(\boldsymbol{r}), \boldsymbol{c}, \boldsymbol{w}). \tag{13}$$

The kinematics of the conformation tensor $\boldsymbol{c}$ is assumed to be given by the bracket (8). Otherwise, its physical interpretation is left unspecified.

Kinematics. The Poisson bracket expressing the kinematics of (13) is derived in [2]. The equations resulting from it governing the nondissipative time evolution of $(\boldsymbol{c}, \boldsymbol{w})$ are the following:

$$\left(\frac{d\boldsymbol{c}}{dt}\right)_{\text{nondiss}} = \boldsymbol{c}\cdot(\nabla\boldsymbol{v} + \Phi_{\boldsymbol{w}}^T) + (\nabla\boldsymbol{v}^T + \Phi_{\boldsymbol{w}})\cdot\boldsymbol{c},$$

$$\left(\frac{d\boldsymbol{w}}{dt}\right)_{\text{nondiss}} = \boldsymbol{w}\cdot(\boldsymbol{\nabla v}+\Phi_{\boldsymbol{w}}^{T})-(\boldsymbol{\nabla v}+\Phi_{\boldsymbol{w}}^{T})\cdot\boldsymbol{w}-2\Phi_{\boldsymbol{c}}\cdot\boldsymbol{c},$$

$$\boldsymbol{\sigma}^{(\text{nd})} = -2\Phi_{\boldsymbol{c}}\cdot\boldsymbol{c}-\Phi_{\boldsymbol{w}}^{T}\cdot\boldsymbol{w}+\boldsymbol{w}\cdot\Phi_{\boldsymbol{w}}^{T}. \tag{14}$$

By comparing (9) with the first equation of (14), we see that $\Phi_{\boldsymbol{w}}$ has indeed the physical meaning of the extra velocity gradient emerging due to the flow-interface interaction.

The above formulation of the active advection has been applied so far only for one specific physical interpretation of $\boldsymbol{c}$: the ellipsoid $r_i c_{ij} r_j = 1$; $\boldsymbol{r}=(r_1,r_2,r_3)\in\boldsymbol{R}^3$ represents a droplet [2,16]. Below, we shall apply it to the Doi-Ohta characterization of the interface morphology.

C. GENERIC formulation of the Doi-Ohta model

The Doi-Ohta model developed in [1] has been put into the form (1) in [11,12]. We shall recall it here.

State variables. The state variables in the Doi-Ohta theory are

$$\boldsymbol{x}=(\boldsymbol{u}(\boldsymbol{r}),\boldsymbol{q},\boldsymbol{Q}). \tag{15}$$

Kinematics. Doi and Ohta derived in [1] the equations representing the passive advection of $(Q,\boldsymbol{q})$ from kinetic theory. It was shown then in [11] that these equations can be cast into the form (5) with the Poisson bracket (8) transformed into state variables $(\boldsymbol{u},\boldsymbol{q},Q)$ by the following transformation:

$$\boldsymbol{u}=\boldsymbol{u},$$

$$\boldsymbol{b}=\boldsymbol{c}^{-1},$$

$$\boldsymbol{b}=Q\boldsymbol{q}+\frac{1}{3}Q^2\boldsymbol{\delta},$$

$$\operatorname{tr}\boldsymbol{q}=0. \tag{16}$$

The inverse of the relation between $\boldsymbol{b}$ and $(\boldsymbol{q},Q)$ given in the second and third equations in (16) is

$$\boldsymbol{q}=\frac{\boldsymbol{b}}{Q}-\frac{1}{3}Q\boldsymbol{\delta},$$

$$Q=(\operatorname{tr}\boldsymbol{b})^{1/2}. \tag{17}$$

The transformation $\boldsymbol{c}\leftrightarrow(\boldsymbol{q},Q)$ introduced in (16) is one to one so that the Poisson bracket (8) expressing kinematics of $(\boldsymbol{u},\boldsymbol{c})$ transforms into a Poisson bracket expressing kinematics of $(\boldsymbol{u},\boldsymbol{q},Q)$ (see more in [11]).

Free energy and dissipation. Doi and Ohta did not introduce the free energy in [1]. By casting their equations into the form (1), the free energy that they in fact used was identified in [11,12]. In the next section we shall combine the Doi-Ohta model with the model of active advection recalled in Sec. II B 2. The free energy, the equations governing the nondissipative time evolution, as well as the dissipative potential and the dissipative time evolution implied by it developed there will reduce to the corresponding quantities in the Doi-Ohta theory by simply omitting the extra variable $\boldsymbol{w}$. We do not have to therefore write down here explicitly the GENERIC form of the governing equations of the original Doi-Ohta theory and we can proceed directly to the extended model.

III. DOI-OHTA MODEL WITH ACTIVE ADVECTION

The Doi-Ohta model is extended by taking into account the active role that the interface and the "rheological inhomogeneity" play in the flow-interface interaction. To formulate the extended model, we combine the state variables (15) of the original Doi-Ohta theory and the state variables used in the active advection model (13). We thus use in this section the following set of *state variables*:

$$x=(\boldsymbol{u}(\boldsymbol{r}),\boldsymbol{q},Q,\boldsymbol{w}). \tag{18}$$

Kinematics. By applying the transformation (16) on the Poisson brackets expressing the kinematics of the Doi-Ohta model [11] [i.e., the bracket (8) transformed into the state variables $(\boldsymbol{u},Q,\boldsymbol{q})$ by (16)] and the active advection model [2] we arrive at the Poisson bracket expressing the kinematics of (18). The equations corresponding to it governing the nondissipative time evolution of (18) are the following:

$$\left(\frac{d\boldsymbol{b}}{dt}\right)_{\text{nondiss}} = -\boldsymbol{b}\cdot(\boldsymbol{\nabla}\Phi_{\boldsymbol{u}}^{T}+\Phi_{\boldsymbol{w}})-(\boldsymbol{\nabla}\Phi_{\boldsymbol{u}}+\Phi_{\boldsymbol{w}}^{T})\cdot\boldsymbol{b},$$

$$\left(\frac{d\boldsymbol{w}}{dt}\right)_{\text{nondiss}} = \boldsymbol{w}\cdot(\boldsymbol{\nabla}\Phi_{\boldsymbol{u}}+\Phi_{\boldsymbol{w}}^{T})-(\boldsymbol{\nabla}\Phi_{\boldsymbol{u}}+\Phi_{\boldsymbol{w}}^{T})\cdot\boldsymbol{w}+2\boldsymbol{b}\cdot\Phi_{\boldsymbol{b}},$$

$$\boldsymbol{\sigma}^{(\text{nd})} = 2\boldsymbol{b}\cdot\Phi_{\boldsymbol{b}}-\Phi_{\boldsymbol{w}}^{T}\cdot\boldsymbol{w}+\boldsymbol{w}\cdot\Phi_{\boldsymbol{w}}^{T}, \tag{19}$$

and finally {we use the free energy (21); note that

$$\Phi_Q=\Gamma-(\Gamma\beta_q/Q^2)\operatorname{tr}(\boldsymbol{q}\cdot\boldsymbol{q})+(\alpha/2)\operatorname{tr}\left[\boldsymbol{w}^T\cdot\boldsymbol{w}\cdot\left(\boldsymbol{q}+\tfrac{2}{3}Q\delta\right)\right],$$

$$\Phi_{\boldsymbol{q}}=(2\Gamma\beta_q/Q)\boldsymbol{q}+(\alpha Q/2)\boldsymbol{w}^T\cdot\boldsymbol{w},$$

and

$$\Phi_{\boldsymbol{w}}=\alpha\boldsymbol{w}\cdot\boldsymbol{b}$$

$$\left(\frac{dQ}{dt}\right)_{\text{nondiss}} = -\operatorname{tr}(\boldsymbol{q}\cdot\boldsymbol{\nabla v}^T)-\frac{\alpha}{Q}\operatorname{tr}(\boldsymbol{b}\cdot\boldsymbol{w}\cdot\boldsymbol{b}),$$

$$\left(\frac{d\boldsymbol{q}}{dt}\right)_{\text{nondiss}} = \left(\frac{\boldsymbol{q}}{Q}+\frac{2}{3}\boldsymbol{\delta}\right)\left(\operatorname{tr}(\boldsymbol{q}\cdot\boldsymbol{\nabla v}^T)+\frac{\alpha}{Q}\operatorname{tr}(\boldsymbol{b}\cdot\boldsymbol{w}\cdot\boldsymbol{b})\right)-\frac{1}{Q}[\boldsymbol{b}\cdot(\boldsymbol{\nabla v}^T+\alpha\boldsymbol{w}\cdot\boldsymbol{b})+(\boldsymbol{\nabla v}+\alpha\boldsymbol{b}\cdot\boldsymbol{w}^T)\cdot\boldsymbol{b}],$$

$$\left(\frac{d\boldsymbol{w}}{dt}\right)_{\text{nondiss}} = \boldsymbol{w}\cdot(\boldsymbol{\nabla v}+\alpha\boldsymbol{b}\cdot\boldsymbol{w}^T)-(\boldsymbol{\nabla v}+\alpha\boldsymbol{b}\cdot\boldsymbol{w}^T)\cdot\boldsymbol{w}+\frac{\boldsymbol{b}}{Q}\left[\left(\Gamma-3\Gamma\beta_q\frac{\operatorname{tr}(\boldsymbol{q}\cdot\boldsymbol{q})}{Q^2}\right)\boldsymbol{\delta}+4\Gamma\beta_q\frac{\boldsymbol{q}}{Q}\right]+\alpha\boldsymbol{b}\cdot\boldsymbol{w}^T\cdot\boldsymbol{w},$$

$$\boldsymbol{\sigma}^{(\mathrm{nd})} = \frac{\boldsymbol{b}}{Q}\left[\left(\Gamma - 3\Gamma\beta_q \frac{\mathrm{tr}(\boldsymbol{q}\cdot\boldsymbol{q})}{Q^2}\right)\boldsymbol{\delta} + 4\Gamma\beta_q \frac{\boldsymbol{q}}{Q}\right] + \alpha \boldsymbol{w}\cdot\boldsymbol{b}\cdot\boldsymbol{w}^T \tag{20}$$

(where $\boldsymbol{v}=\Phi_{\boldsymbol{u}}=\boldsymbol{u}/\rho$).

Free energy

$$\Phi = \Phi^{(\mathrm{kin})} + \Phi^{(\mathrm{interface})} + \Phi^{(\mathrm{shape})}, \tag{21}$$

$$\Phi^{(\mathrm{kin})} = \int d\boldsymbol{r}\left(\frac{\boldsymbol{u}^2}{2\rho} + \frac{\alpha}{2}\mathrm{tr}(\boldsymbol{w}^T\cdot\boldsymbol{b}\cdot\boldsymbol{w})\right), \tag{22}$$

$$\Phi^{(\mathrm{interface})} = \int d\boldsymbol{r}\,\Gamma Q, \tag{23}$$

$$\Phi^{(\mathrm{shape})} = \int d\boldsymbol{r}\frac{\Gamma\beta_q \mathrm{tr}(\boldsymbol{q}\cdot\boldsymbol{q})}{Q}. \tag{24}$$

The physical meaning of the four terms and the three material parameters (α,Γ,β_q) introduced in (21) will be discussed in Secs. III A and III B.

Dissipation potential. The thermodynamic forces that drive the immiscible blend to equilibrium are the following:

$$X^{(1)} = \Phi_Q,$$

$$\boldsymbol{X}^{(2)} = \Phi_{\boldsymbol{q}},$$

$$\boldsymbol{X}^{(3)} = \Phi_{\boldsymbol{w}},$$

$$\boldsymbol{X}^{(4)} = \boldsymbol{D}, \tag{25}$$

where $\boldsymbol{D}=\frac{1}{2}(\boldsymbol{\nabla v}+\boldsymbol{\nabla v}^T)$.

From these thermodynamic forces we now construct a dissipation potential satisfying the general properties (2). If we restrict ourselves to states at which the thermodynamic forces (25) are not too large, it suffices to consider the following quadratic potential:

$$\Xi = \int d\boldsymbol{r}\frac{1}{2}\left[\Lambda^{(1)}(X^{(1)})^2 + \Lambda^{(2)}X^{(2)}_{ij}X^{(2)}_{ij} + (X^{(3)}_{ij},\ X^{(4)}_{ij})\times\begin{pmatrix}\Lambda^{(3)}_{jk} & \Lambda^{(4)}_{jk}\\ \Lambda^{(4)}_{jk} & \eta_0\delta_{jk}\end{pmatrix}\begin{pmatrix}X^{(3)}_{ik}\\ X^{(4)}_{ik}\end{pmatrix}\right], \tag{26}$$

where $\Lambda^{(1)}>0$, $\Lambda^{(2)}>0$, and $\begin{pmatrix}\Lambda^{(3)} & \Lambda^{(4)}\\ \Lambda^{(4)} & \eta_0\boldsymbol{\delta}\end{pmatrix}>0$ are dissipative phenomenological coefficients. They can depend on the state variables $(\boldsymbol{u},\boldsymbol{q},Q,\boldsymbol{w})$ but are independent of $(\Phi_{\boldsymbol{u}},\Phi_{\boldsymbol{q}},\Phi_Q,\Phi_{\boldsymbol{w}})$.

The equations governing the dissipative time evolution (6) implied by (26) are the following:

$$\left(\frac{dQ}{dt}\right)_{\mathrm{diss}} = -\frac{\delta\Xi}{\delta\Phi_Q} = -\Lambda^{(1)}\Phi_Q,$$

$$\left(\frac{dq_{ij}}{dt}\right)_{\mathrm{diss}} = -\frac{\delta\Xi}{\delta\Phi_{q_{ij}}} = -\Lambda^{(2)}\Phi_{q_{ij}},$$

$$\left(\frac{dw_{ij}}{dt}\right)_{\mathrm{diss}} = -\frac{\delta\Xi}{\delta\Phi_{w_{ij}}} = -\Phi_{w_{ik}}\Lambda^{(3)}_{kj} - \frac{1}{2}(D_{ik}\Lambda^{(4)}_{kj} + \Lambda^{(4)}_{ik}D_{kj}). \tag{27}$$

We now proceed to specify more clearly the coefficients introduced in the dissipation potential (26):

$$\Lambda^{(1)} = \frac{d_1 Q}{\eta_0}[\mathrm{tr}(\boldsymbol{q}\cdot\boldsymbol{q})]^{1/2}$$

$$\Lambda^{(2)} = \frac{d_1 Q^2}{2\beta_q\eta_0}\left[\left(\frac{1}{\mu}-1\right)Q + [\mathrm{tr}(\boldsymbol{q}\cdot\boldsymbol{q})]^{1/2}\right],$$

$$\boldsymbol{\Lambda}^{(3)} = \lambda\boldsymbol{b}^{-1},$$

$$\boldsymbol{\Lambda}^{(4)} = \xi\boldsymbol{b}^{-1}. \tag{28}$$

The first two have been chosen in such a way that we recover with them (by ignoring $\boldsymbol{w}$) the original Doi-Ohta theory; $\mu = d_1/(d_1+d_2)$, $d_1>0$ and $d_2>0$ (denoted c_1 and c_2 in the Doi-Ohta paper) are phenomenological parameters, and η_0 is the viscosity coefficient. The third and the fourth coefficients $\Lambda^{(3)}$ are $\Lambda^{(4)}$ are new. We shall discuss their physical interpretation in Sec. III B

With the choices (28) and (21), the dissipative time evolution equations (27) become

$$\left(\frac{dQ}{dt}\right)_{\mathrm{diss}} = -\frac{d_1\Gamma Q}{\eta_0}[\mathrm{tr}(\boldsymbol{q}\cdot\boldsymbol{q})]^{1/2} + \frac{d_1\beta_q\Gamma}{\eta_0 Q}[\mathrm{tr}(\boldsymbol{q}\cdot\boldsymbol{q})]^{3/2} - \frac{d_1\alpha Q}{2\eta_0}[\mathrm{tr}(\boldsymbol{q}\cdot\boldsymbol{q})]^{1/2}\mathrm{tr}\left[\boldsymbol{w}^T\cdot\boldsymbol{w}\cdot\left(\boldsymbol{q}+\frac{2}{3}Q\boldsymbol{\delta}\right)\right],$$

$$\left(\frac{d\boldsymbol{q}}{dt}\right)_{\mathrm{diss}} = -\frac{d_1}{\eta_0}\left[\left(\frac{1}{\mu}-1\right)Q + [\mathrm{tr}(\boldsymbol{q}\cdot\boldsymbol{q})]^{1/2}\right]\times\left(\Gamma\boldsymbol{q} + \frac{\alpha Q^2}{4\beta_q}\boldsymbol{w}^T\cdot\boldsymbol{w}\right),$$

$$\left(\frac{d\boldsymbol{w}}{dt}\right)_{\mathrm{diss}} = -\alpha\lambda\boldsymbol{w} - \xi\boldsymbol{D}\cdot\boldsymbol{b}^{-1}. \tag{29}$$

Summing up, the governing equations of the extended Doi-Ohta model are (4), (20), and (29). It is easy to verify that, by omitting $\boldsymbol{w}$, the governing equations of the original Doi-Ohta model are indeed recovered except for two additional terms (one quadratic and one third order in $\boldsymbol{q}$), appearing in our formulation, in the expression for the extra stress tensor. We emphasize at this point that all the terms in the free energy, including in particular the term $\Phi^{(\mathrm{shape})}$, are essential for casting the original Doi-Ohta equations into the GENERIC form. In other words we have shown that the Doi-Ohta theory is compatible with thermodynamics only if the free energy is given by (21). Doi and Ohta did not introduce the free energy explicitly in [1] since they derived their equations in a different way than we did, and they did not investigate the problem of the compatibility with thermodynamics. As shown in [11] and also in this paper, the free energy they use implicitly is (21) with $\boldsymbol{w}=\boldsymbol{0}$.

A. Physics expressed in the governing equations

Having written the time evolution equations, we now discuss in more detail the physics expressed in them. This discussion will also throw light on the physical interpretation of the state variables (18).

1. u

We begin with the field $\boldsymbol{u}$. The motion of a continuum is seen in all approaches to the physics of continuum as a one-parameter family of transformations $\mathbf{R}^3 \rightarrow \mathbf{R}^3$. These transformations form a Lie group. The kinematics of the continuum is expressed mathematically as a structure of this Lie group. The Poisson bracket associated canonically with the dual of the Lie algebra corresponding to this Lie group is given (see [14,15]) by the first line in (8); $\boldsymbol{u}$ is an element of the dual of the Lie algebra. We thus conclude that the kinematics that we have used for the field $\boldsymbol{u}$ implies that $\boldsymbol{u}$ has the physical interpretation of the overall momentum field of the fluid. This interpretation is then also consistent with interpreting the first term in the (22) as the overall kinetic energy.

We note here that in mechanics as well as in thermodynamics the state variables are always accompanied by their conjugates (in our case the conjugate of a state variable is a derivative of the free energy with respect to the state variables). The conjugate of the field $\boldsymbol{u}$ is thus $\Phi_{\boldsymbol{u}}=\boldsymbol{u}/\rho=\boldsymbol{v}$, where $\boldsymbol{v}$ the velocity field. It is the field $\boldsymbol{v}$ that is directly measured in hydrodynamic experiments and it is therefore the state variable preferred in classical hydrodynamics. We use $\boldsymbol{u}$, which has a less direct physical interpretation since it is with $\boldsymbol{u}$ that the Hamiltonian structure of fluid mechanics is clearly displayed. We recall that the same observation can be made about many other pairs of state variables. For example, the temperature is a directly measurable quantity in thermodynamics but it is advantageous to use its conjugate (i.e., the internal energy which is not directly measurable) as preferred state variable if we want to display and use the mathematical structure of thermodynamics.

2. w

We recall a few observations about the Stokes problem.

(i) The mathematical formulation of the Stokes problem consists of the Navier-Stokes equation for the flow velocity with the outer boundary condition being the given imposed velocity and the inner boundary condition expressing the bulk-interface interaction. The solution depends on time explicitly and implicitly: explicitly because the Navier-Stokes equation is the time evolution equation and implicitly through the time dependence involved in the inner boundary condition. The explicit time dependence is usually neglected by replacing the full Navier-Stokes equation with its stationary creeping flow approximation.

(ii) The advection of the interface is modified by replacing $\nabla \boldsymbol{v}$ on the right-hand side of the second equation in (9) by $\nabla \boldsymbol{v}+\boldsymbol{\epsilon}$, where $\boldsymbol{\epsilon}$ is the gradient of the velocity perturbation.

How shall we formulate the Stokes problem in the mesoscopic setting used in this paper? We certainly cannot formulate the inner boundary condition since the knowledge of the exact shape and precise location of the interface, needed in the formulation, is outside the scope of the mesoscopic description. We shall proceed as follows: We look for a modification of the advection in which $\nabla \boldsymbol{v}$ on the right-hand side of the second equation in (9) is replaced by $\nabla \boldsymbol{v}+\boldsymbol{\epsilon}$, where the time evolution of $\boldsymbol{\epsilon}$ is coupled to the time evolution of the rest of the state variables in such a way that together the time evolution is GENERIC. The latter requirement means that the GENERIC nature of the original formulation of the Stokes problem (and thus all the physics expressed in this structure; see Sec. II A) is preserved. The problem that we are facing can also be formulated (in a more mathematical language) as follows: We look for an extension (deformation) of (7) and (9) in which $\nabla \boldsymbol{v}$ on the right-hand side of the second equation in (9) deforms into $\nabla \boldsymbol{u}+\boldsymbol{\epsilon}$ and the Poisson bracket (8) deforms into a new Poisson bracket involving $\boldsymbol{\epsilon}$.

The setting presented in Eqs. (13) and (14) provides a solution to this problem. It may not be, however, a unique solution. We have been unable to prove the uniqueness but we have also been unable to find another solution.

The way $\boldsymbol{w}$ appears in (19) shows that the transpose of the conjugate of $\boldsymbol{w}$ has the physical interpretation of the gradient of the velocity perturbation. We thus interpret the second term in (22) as the contribution of the velocity perturbation to the kinetic energy. We shall take the parameter α to be the inverse of the average mass of the blend.

In contrast to the microhydrodynamic formulation of the Stokes problem we keep in its mesoscopic formulation the explicit time dependence of the perturbed velocity. This is consistent with a general observation that, when passing from microscopic to more macroscopic levels of description, we deal with larger objects, and thus the effect of inertia becomes more important. Moreover, if we want to preserve the GENERIC structure with $\boldsymbol{w}$, we have to keep the time evolution of $\boldsymbol{w}$.

Originally, we regard all three state variables $(\boldsymbol{u},\boldsymbol{c},\boldsymbol{w})$ as slow variables, their time evolution is assumed to be separated from the time evolution of the fast time evolution of irrelevant microscopic details. Let us now assume that the relaxation time of $\boldsymbol{w}$ is very small (as we do later in the comparison with results of experimental observations) and thus $\boldsymbol{w}$ becomes a fast variable. What this means is that $\boldsymbol{w}$ becomes in fact a function of the slow variables (in other words, $\boldsymbol{w}$ becomes enslaved to the remaining slow variables). It can be thus considered as a fast variable, separated from the slow variables, and omitted. The separation brings about then a change of the slow time evolution; namely, the affine advection [i.e., the advection without $\Phi_{\boldsymbol{w}}^T$ in the first two terms on the right-hand side of the first equation in (19)] becomes the nonaffine advection [i.e., $\Phi_{\boldsymbol{w}}^T$ in the first two terms on the right-hand side of the first equation in (19) becomes a function of $\nabla \Phi_{\boldsymbol{u}}$; see more in [2]]. In this paper we shall not make the separation even in the case when the relaxation time of $\boldsymbol{w}$ is very small (see Sec. IV) because such elimination leads to the time evolution equations that do no longer possess the GENERIC structure.

3. (Q,q)

It has been established in [11] that the kinematics expressed in the Poisson bracket obtained by transforming [us-

ing the transformation (16)] the Poisson bracket (8) is the same as the kinematics derived (implicitly) in [1]. Moreover, in order to interpret (23) as the surface tension contribution to the free energy, Q has to have the interpretation of the area of the interface per unit volume. We thus conclude that $(Q,\boldsymbol{q})$ have the same physical interpretation as $(Q,\boldsymbol{q})$ introduced in [1].

Doi and Ohta relate $(Q,\boldsymbol{q})$ to the second moment of the one-particle distribution function $f(\boldsymbol{r},\boldsymbol{n})$, where $\boldsymbol{n}$ is the unit vector perpendicular to the tangent plane of the interface at the point $\boldsymbol{r}$. The tensor $\boldsymbol{q}$ is the traceless part of the second moment in $\boldsymbol{n}$. In what sense does the tensor $\boldsymbol{q}$ characterize the shape of the interface? The tensor $\boldsymbol{q}$ is certainly related to the anisotropy of the interface distribution and thus indirectly also to its deformations. Indeed, $\boldsymbol{q}=\boldsymbol{0}$ implies that the distribution is isotropic. It is also clear that $\boldsymbol{q}$ is not directly related to the curvature. Note that the distribution function $f(\boldsymbol{r},\boldsymbol{n})$ itself does not contain any direct information about the curvature. For that being the case we would have to know how $\boldsymbol{n}$ changes under the infinitesimal displacement of the point to which it is attached. Indirectly, however, $\boldsymbol{q}$ does characterize anisotropy of the distribution of $\boldsymbol{n}$ and thus also (very indirectly) the curvature.

4. Other state variables

The questions that have to be asked in any mesoscopic theory are the following: Are the state variables well chosen? Does the time evolution described in the theory represent the most pertinent part of the time evolution, does it indeed represent the slow time evolution that is well separated from the fast time evolution representing the impertinent details? These questions can be answered by either deriving the mesoscopic theory from a more microscopic theory or by comparing consequences of the mesoscopic theory with results of experimental observations. Below, we shall make only a few comments about possible additional state variables that can be adopted to improve the theory. The derivation from a more microscopic theory is out of the scope of this paper, the comparison with other theories and with experiments is presented in Sec. IV.

As shown in [17] and in the references cited therein, the free energy $\Phi^{(\text{inter face})}$ representing the surface tension contribution to the free energy should include also terms [that are added to (23)] involving the curvature of the interface. In order to be able to write down such terms we would have to adopt new state variables with which the curvature can be expressed. For the specific blends discussed in Sec. IV the curvature-dependent contribution to the free energy is, as follows from [17], very small and we therefore do not pursue this route in this paper.

In the case when the interface is a membrane with its own internal mechanical (elastic) properties then the free energy has to include terms expressing the membrane elastic energy (see, e.g., [18]). To be able to write down such terms, we would have to again enlarge the set of state variables by adopting new ones allowing to express the curvature and elastic deformations (including stretching) of the interface. We hope to follow this route in a future presentation but in this paper we limit ourselves (see Sec. IV) to the interfaces with very small or totally absent elastic deformations and we therefore do not need to make such extensions.

The morphological state variables $(Q,\boldsymbol{q})$ describe the morphology locally. We may expect that the global (shape) features of the interface (for example, the size and the distribution of droplets or the co-continuous form of the interface) play an important role in determining the overall free energy (in particular in determining its entropic part). Let the state variables through which the global shape of the interface can be expressed be denoted by the symbol $x^{(\text{shape})}$. Let us assume that we formulate an extended theory involving $x^{(\text{shape})}$ and thus we have equations governing the time evolution of $x^{(\text{shape})}$. Let this time evolution be faster than the time evolution of the rest of state variables and thus $x^{(\text{shape})}$ becomes enslaved to them [i.e., $x^{(\text{shape})}$ becomes a function of $(Q,\boldsymbol{q})$]. We suggest that the free energy (24) is the part of the free energy representing the global shape contribution depending after $x^{(\text{shape})}$ on which it depends has been replaced by $x^{(\text{shape})(Q,\boldsymbol{q})}$, on $(Q,\boldsymbol{q})$. We thus interpret (24) as an approximation to the shape-dependent free energy. The coefficient β_q introduced in it is considered as a (dimensionless) phenomenological material parameter [see more in Sec. IV B, Eq. (52)].

We recall that we have seen in Sec. III [see the text following Eq. (29)] that the part of the free energy proportional to β_q is essential for casting the original Doi-Ohta equations into the GENERIC form. Specifically, it is essential for obtaining the dissipative part of the time evolution. Only with this term in the free energy the inequality $(\partial\Phi/\partial t)_{\text{dissip}}<0$ is guaranteed. We note here that in order to guarantee $\partial\Phi/\partial t=(\partial\Phi/\partial t)_{\text{nondissip}}+(\partial\Phi/\partial t)_{\text{dissip}}<0$ we need to guarantee that $(\partial\Phi/\partial t)_{\text{nondissip}}=0$. This is indeed guaranteed provided the extra stress tensor is given by the last equation in (20). The terms involving β_q are, however, missing in the expression for the stress tensor used in the original Doi-Ohta models (this has been noted already in [11]). We shall see in Sec. IV that the missing terms improve the rheological predictions of the model.

B. Material parameters

Every theory, formulated on any level of description, needs parameters (called material parameters) expressing the individual features of the systems under consideration. For instance, in classical mechanics, it is the mass and all the parameters entering the characterization of the forces, in hydrodynamics of simple fluids, the material parameters are the viscosity and the heat conductivity coefficients and all the parameters entering the local fundamental thermodynamic relation. The mapping: *physical systems*$\rightarrow$*material parameters* can be obtained by following two routes: route 1, by staying inside the level, or route 2, by investigating relations to other levels. Below, we shall make a few brief comments about both routes.

Route 1. Let the level on which we place ourselves be denoted by the symbol $\mathcal{L}_0$. Among all experimental observations made on the level $\mathcal{L}_0$ (we shall denote them by the symbol $\mathcal{O}_0$) we select some $(\mathcal{O}_0^{\text{metr}}\subset\mathcal{O}_0)$ that will be regarded as measurements of the material parameters. The val-

ues of the parameters are obtained by fitting the results of the observations $\mathcal{O}_0^{\text{metr}}$ with predictions of the theory. The success or the failure of the theory is then seen in the comparison of the results of the remaining $\mathcal{O}_0 \backslash \mathcal{O}_0^{\text{metr}}$ observations with predictions of the theory. This route is traditionally followed on all well-established levels as for example in classical thermodynamics, classical mechanics, and classical hydrodynamics.

Route 2. Let the level $\mathcal{L}_1$ be more microscopic (i.e., involving more details) than the level $\mathcal{L}_0$. For instance, let $\mathcal{L}_0$ be the level of classical hydrodynamics and $\mathcal{L}_1$ the level of Boltzmann kinetic theory. Both levels $\mathcal{L}_0$ and $\mathcal{L}_1$ are autonomous (i.e., neither of them needs the other to be formulated and applied) but since the level $\mathcal{L}_1$ is more microscopic we can anticipate that an analysis of solutions of the governing equations on the level $\mathcal{L}_1$ can lead to a derivation of the theory on the level $\mathcal{L}_0$. The process of the derivation can be seen as a pattern recognition process in the set of solutions (trajectories) obtained on the level $\mathcal{L}_1$. For instance, in the case of $\mathcal{L}_1$ being the Boltzmann kinetic theory and $\mathcal{L}_0$ the hydrodynamics, such passage $\mathcal{L}_1 \rightarrow \mathcal{L}_0$ is provided by the famous Chapman-Enskog method. Let the material parameters associated with the level $\mathcal{L}_1$ ($\mathcal{L}_0$) be denoted $\mathcal{P}_1$ ($\mathcal{P}_1$). The passage $\mathcal{L}_1 \rightarrow \mathcal{L}_0$ induces the passage $\mathcal{P}_1 \rightarrow \mathcal{P}_0$. The material parameters $\mathcal{P}_0$ can be thus obtained by independent measurements made on the level $\mathcal{L}_1$. For example, by using the Chapman-Enskog method, we obtain the viscosity and the heat conductivity coefficients expressed in terms of the material parameters used in the Boltzmann kinetic theory.

Now, let the level $\mathcal{L}_0$ (we shall denote it hereafter $\mathcal{L}_{\text{meso}}$) be the level with the state variables (18) and the governing equations (20) and (27) and the more microscopic level $\mathcal{L}_1$ (denoted hereafter $\mathcal{L}_{\text{microhyd}}$) the level of microhydrodynamics on which the interface is specified as a surface in $\mathbf{R}^3$, i.e., as an immersion $\mathbf{R}^2 \supset \Omega \hookrightarrow \mathbf{R}^3$. The material parameters used on the level $\mathcal{L}_{\text{meso}}$ are

$$(d_1, \mu, \eta_0, \Gamma, \beta_q, \lambda, \xi). \tag{30}$$

The first four appear already in the original Doi-Ohta theory; the last three are new. We emphasize that all these material parameters have a clear physical interpretation from the way they have appeared in the GENERIC construction of the governing equations. Essentially, they quantify the physics that we have introduced into our model. We also note that all the parameters that entered the dissipation potential (i.e., $d_1, \mu, \eta_0, \lambda, \xi$) do not have to be just numbers, they can be functions of the state variables. We have to require only that the properties of the dissipation potential (2) hold.

The material parameters serving on the level of microhydrodynamics are the hydrodynamic parameters characterizing the two fluids involved as well as the parameters characterizing their interface and the bulk-interface interactions.

Some material parameters included in (30) will be determined in Sec. IV by following route 2, some by following route 1. We recall briefly the way we proceeded in [16]. The morphology of the interface in [16] is seen as a collection of droplets mathematically described as ellipsoids. If we then limit ourselves to small deformations we can solve (by using the perturbation method) both the microhydrodynamic formulation and the mesoscopic formulation analytically. By comparing the solutions we find the mapping $\mathcal{P}_{\text{microhyd}} \rightarrow \mathcal{P}_{\text{meso}}$. We shall follow a similar strategy in Sec. IV.

Before identifying the material parameters (30) for the blends observed in experiments we explore solutions to the governing equations for a large domain of the parameters. Already this investigation allows us to identify regions in the space of material parameters that have to be excluded. For example, we find in the next section that if $\lambda < 10^8$ than the solutions are unphysical (they oscillate widely in time and do not reach stationary values).

Finally, we comment about the choice of the coefficient Λ_1 that we have made [following [1], in (28)]. The advantage of this particular choice is that the relaxation of Q stops once the isotropic distribution of the interface (corresponding to $\mathbf{q}=\mathbf{0}$) is reached. This is indeed the behavior observed in experiments. We recall (see, e.g., [19]) that in the physical systems involving an interface endowed with surface tension the extra stress (determined for example, in the case of spherical droplets, by the well-known Young-Laplace formula) remains to be present even at the complete equilibrium. In the next section, where we shall calculate rheological consequences of the governing equations, we shall also mention other choices for the coefficients $\Lambda^{(1)}$, $\Lambda^{(2)}$, $\Lambda^{(3)}$, and compare their consequences.

IV. RESULTS

Now we proceed to solve Eqs. (4), (20), and (29). From the mathematical point of view, they represent a set of ordinary differential equations that we solve numerically by using standard software packages. In the cases when the equations are "stiff," we use the solver called ODE23S in MATLAB. It is based on a modified Resenbrock formula of order 2.

We solve the equations with the imposed flow being a simple shear flow. From the calculated extra stress tensor we extract the standard rheological characteristics and present them in figures. The initial condition in our calculations is always

$$Q = Q_0, \quad \boldsymbol{q} = \mathbf{0}, \quad \boldsymbol{w} = \mathbf{0}, \tag{31}$$

where Q_0 is considered to be a parameter.

The predictions of the active Doi-Ohta (DO) model [i.e., for Eqs. (4), (20), and (29)] will be compared below with predictions of some other models and some published experimental data. The other models that we shall consider are four Doi-Ohta-type models [denoted as DO1, DO2, Lee-Park (LP), and Wagner-Ottinger Edwards (WOE) models] and one [the Frankel-Acrivos (FA) model] based on an approximate (small deformation) microhydrodynamic analysis. The Doi-Ohta-type models all share the same nondissipative time evolution [governed by (20) with $\boldsymbol{w}$ missing] and differ in the choice of the dissipative coefficients Λ_1 and Λ_2. They are the following.

DO1 model. This is the original Doi-Ohta model [1] (i.e., the field $\boldsymbol{w}$ is absent) corresponding to $\Lambda^{(1)}$ and $\Lambda^{(2)}$ given in (28) with $\text{tr}(\boldsymbol{q}\cdot\boldsymbol{q})$ replaced by Q^2 (also used in [26,28]).

DO2 model. This is the original Doi-Ohta model [1] (i.e., the field $\boldsymbol{w}$ is absent) corresponding to Λ_1 and Λ_2 given in (28) (also used in [27]).

LP model. This is the modification of the Doi-Ohta model introduced by Lee and Park [20]. In their reinterpretation of the physics involved in the dissipative time evolution, d_1 is the rate coefficient of droplet coalescence, d_2 is the rate coefficient of the shape relaxation, and a new parameter, d_3, is the rate of droplet break up and deformations.

WOE model. This is the modification of the Doi-Ohta model introduced in [21]. In this model the initial value of Q, namely, Q_0, plays the role of the length scale. The thermodynamic force driving Q to equilibrium is proportional to $Q-Q_0$.

FA model. This is not a model formulated on a mesoscopic level as the previous four are. The immiscible blend is assumed to be a colloidal suspension of spherical droplets that only slightly change their shape in the flow. With this assumption, the microhydrodynamic formulation [22] of the dynamics of the interface can be brought into closed form expressions for quantities characterizing rheological behavior [22,23]. In Ref. [23] the droplet radius is allowed to depend on the shear rate.

A. Dimensionless equations

We recall that an immiscible blend is regarded on the mesoscopic level that we have adopted in this paper as a single fluid with an internal structure. In view of the experimental data with which we shall later compare predictions of the model, we shall hereafter restrict ourselves to the droplet morphology. The single fluid will be the fluid outside the droplets and the surface of the droplets will be the internal structure. Instead of η_0 denoting the viscosity of the single fluid we shall now use η_{out}.

We shall regard $1/Q_0$ as a characteristic length (Q_0 is the initial surface area per unit volume of the interface), $\eta_{\text{out}}/(Q_0\Gamma)$ as the characteristic time, and Γ is the surface tension. We note that in the particular case of suspensions of spherical droplets, $Q_0=3\phi/r_0$, where r_0 is the initial radius of the droplet and ϕ the volume fraction of the droplets. The dimensionless state variables are introduced as follows:

$$Q^* = \frac{Q}{Q_0},\ \boldsymbol{q}^* = \frac{\boldsymbol{q}}{Q_0},$$

$$t^* = t\frac{Q_0\Gamma}{\eta_{\text{out}}},\quad \boldsymbol{\nabla v}^* = \frac{\boldsymbol{\nabla v}}{\dot\gamma},\quad \boldsymbol{w}^* = \frac{\boldsymbol{w}}{\eta_{\text{out}}},\quad \sigma^* = \frac{\sigma}{\eta_{\text{out}}\dot\gamma}. \tag{32}$$

The dimensionless time evolution equations become (in order to simplify the notation we omit hereafter the superscript $*$; all quantities are dimensionless)

$$\frac{dQ}{dt} = -\mathcal{C}\,\mathrm{tr}(\boldsymbol{q}\cdot\boldsymbol{\nabla}v^T) - \kappa\frac{\mathrm{tr}(\boldsymbol{b}\cdot\boldsymbol{w}\cdot\boldsymbol{b})}{Q} - d_1\left\{(\boldsymbol{q}:\boldsymbol{q})^{1/2}Q - \beta_q\frac{(\boldsymbol{q}:\boldsymbol{q})^{3/2}}{Q} + \frac{\kappa}{2}Q(\boldsymbol{q}:\boldsymbol{q})^{1/2}\mathrm{tr}\left[\boldsymbol{w}^T\cdot\boldsymbol{w}\cdot\left(\boldsymbol{q}+\frac{2}{3}Q\boldsymbol{\delta}\right)\right]\right\},$$

$$\frac{d\boldsymbol{q}}{dt} = \left(\frac{\boldsymbol{q}}{Q}+\frac{2}{3}\boldsymbol{\delta}\right)\left(\mathcal{C}\,\mathrm{tr}(\boldsymbol{q}\cdot\boldsymbol{\nabla}v^T) + \kappa\frac{\mathrm{tr}(\boldsymbol{b}\cdot\boldsymbol{w}\cdot\boldsymbol{b})}{Q}\right) - \frac{1}{Q}[\mathcal{C}(\boldsymbol{b}\cdot\boldsymbol{\nabla}\boldsymbol{v}^T+\boldsymbol{\nabla}\boldsymbol{v}\cdot\boldsymbol{b}) + \kappa\boldsymbol{b}\cdot(\boldsymbol{w}+\boldsymbol{w}^T)\cdot\boldsymbol{b}] - d_1\left[\left(\frac{1}{\mu}-1\right)Q + (\boldsymbol{q}:\boldsymbol{q})^{1/2}\right]\left(\boldsymbol{q}+\frac{\kappa}{4\beta_q}Q^2\boldsymbol{w}^T\cdot\boldsymbol{w}\right),$$

$$\frac{d\boldsymbol{w}}{dt} = \mathcal{C}(\boldsymbol{w}\cdot\boldsymbol{\nabla}\boldsymbol{v}-\boldsymbol{\nabla}\boldsymbol{v}\cdot\boldsymbol{w}) + \kappa(\boldsymbol{w}\cdot\boldsymbol{b}\cdot\boldsymbol{w}^T-\boldsymbol{b}\cdot\boldsymbol{w}^T\cdot\boldsymbol{w}) + \frac{\boldsymbol{b}}{Q}\cdot\left[\left(1-3\beta_q\frac{\boldsymbol{q}:\boldsymbol{q}}{Q^2}\right)\boldsymbol{\delta}+4\beta_q\frac{\boldsymbol{q}}{Q}\right] + \kappa\boldsymbol{b}\cdot\boldsymbol{w}^T\cdot\boldsymbol{w} - \mu_1\boldsymbol{w} - \mathcal{C}\mu_2\boldsymbol{D}\cdot\boldsymbol{b}^{-1},$$

$$\boldsymbol{\sigma}^{\text{int}} = \mathcal{C}^{-1}\left\{\frac{\boldsymbol{b}}{Q}\cdot\left[\left(1-3\beta_q\frac{\boldsymbol{q}:\boldsymbol{q}}{Q^2}\right)\boldsymbol{\delta}+4\beta_q\frac{\boldsymbol{q}}{Q}\right] + \kappa\boldsymbol{w}\cdot\boldsymbol{b}\cdot\boldsymbol{w}^T\right\}, \tag{33}$$

where

$$\boldsymbol{b} = Q\boldsymbol{q} + \frac{1}{3}Q^2\boldsymbol{\delta}. \tag{34}$$

The dimensionless parameters appearing in (32) are defined as follows:

$$\mathcal{C} = \frac{\eta_{\text{out}}\dot\gamma}{Q_0\Gamma},\quad \kappa = \frac{\alpha Q_0\eta_{\text{out}}^2}{\Gamma},\quad \mu_1 = \frac{\lambda\alpha\eta_{\text{out}}}{Q_0\Gamma},\quad \mu_2 = \frac{\xi}{Q^2\eta_{\text{out}}}. \tag{35}$$

The dimensionless parameter $\mathcal{C}$ is a capillary number describing the relative strength of the applied viscous force (which tends to enlarge and deform the interface) to that of the interfacial tension (which tends to resist the deformations). The dimensionless parameter κ, representing the ratio of the kinetic energy of the interface to the interfacial free energy, is a known parameter since α is the inverse of mass density of the interface. The parameters d_1 and μ are the same as those introduced in the original Doi-Ohta model. The dimensionless parameters μ_1 and μ_2 characterize the dissipation of $\boldsymbol{w}$. They, as well as β_q, will be determined (see Sec. IV B) by relating particular solutions of the present model to those arising in the the microhydrodynamic formulation.

The initial conditions are the following:

$$Q=1,\quad \boldsymbol{q}=\boldsymbol{0},\quad \boldsymbol{w}=\boldsymbol{0}. \tag{36}$$

B. Determination of the material parameters

The dimensionless parameters appearing in (32) are

$$(d_1,\mu,\beta_q,\mu_1,\mu_2). \tag{37}$$

The first two were introduced in the original Doi-Ohta theory (see [1]); β_q, μ_1, and μ_2 are new material parameters. In this section, the new parameters will be determined, i.e., they will be expressed in terms of the remaining material param-

eters. The method we use is similar to the one used in [16]. We solve analytically the equations of the present model in a particular situation and compare them with the analytical solutions of the microhydrodynamic equations in the same situation. The particular situation that we consider corresponds to the weak external flow. The equations, both those arising in the mesoscopic model and those arising in the microhydrodynamic formulation, are solved by the perturbation method with the capillary number $\mathcal{C}$ playing the role of the small parameter:

$$Q = 1 + \mathcal{C}Q^{(1)} + O(\mathcal{C}^2), \tag{38}$$

$$\boldsymbol{q} = \mathcal{C}\boldsymbol{q}^{(1)} + O(\mathcal{C}^2), \tag{39}$$

and

$$\boldsymbol{w} = \mathcal{C}\boldsymbol{w}^{(1)} + O(\mathcal{C}^2). \tag{40}$$

We assume moreover that $\boldsymbol{w}$ evolves in time much faster than Q and $\boldsymbol{q}$. To first order in the small parameter $\mathcal{C}$, Eqs. (33) become

$$\frac{dQ^{(1)}}{dt} = -d_1(\boldsymbol{q}^{(1)}:\boldsymbol{q}^{(1)})^{1/2}, \tag{41}$$

$$\frac{d\boldsymbol{q}^{(1)}}{dt} = -\frac{2}{3}\left(1 - \frac{\kappa\mu_2}{\mu_1}\right)\boldsymbol{D} - \left[\left(\frac{1}{\mu} - 1\right)d_1 + \frac{2\kappa}{27\mu_1}(4\beta_q + 3)\right]\boldsymbol{q}^{(1)}, \tag{42}$$

$$\boldsymbol{w}^{(1)} = \frac{1}{\mu_1}\left[\left(\frac{4}{3}\beta_q + 1\right)\boldsymbol{q}^{(1)} - 3\mu_2\boldsymbol{D}\right], \tag{43}$$

and the interfacial excess stress tensor is written as

$$\boldsymbol{\sigma}^{\text{int}} = \left(\frac{4}{3}\beta_q + 1\right)\boldsymbol{q}^{(1)} + O(\mathcal{C}). \tag{44}$$

From Eq. (42) we obtain the relaxation time of $\boldsymbol{q}$ (with dimension) as

$$\tau_q = \frac{\eta_{\text{out}}}{Q_0\Gamma}\frac{1}{(1/\mu - 1)d_1 + (2\kappa/27\mu_1)(4\beta_q + 3)}. \tag{45}$$

At the steady state, with $d\boldsymbol{q}^{(1)}/dt = \boldsymbol{0}$, Eq. (44) leads to the following zero-shear viscosity:

$$[-\sigma_{12}^{\text{int}}]_0 = \frac{(1 - \kappa\mu_2/\mu_1)(4\beta_q + 3)}{9[(1/\mu - 1)d_1 + (2\kappa/27\mu_1)(4\beta_q + 3)]}. \tag{46}$$

Now, we turn to the analytical solutions known from microhydrodynamic theories for the problem of emulsions. First, we compare the stresses. Taylor's small deformation theory [24] leads to

$$[\eta^{\text{int}}]_0 = \frac{5p + 2}{2p + 2}, \tag{47}$$

where $p = \eta_{\text{in}}/\eta_{\text{out}}$, and η_{in} (η_{out}) is the viscosity coefficient of the fluid inside (outside) the droplet. By equating (46) with (47) we arrive at the first equation relating the microhydrodynamic material parameters and (37):

$$\frac{(1 - \kappa\mu_2/\mu_1)(4\beta_q + 3)}{9[(1/\mu - 1)d_1 + (2\kappa/27\mu_1)(4\beta_q + 3)]} = \frac{5p + 2}{2p + 2}. \tag{48}$$

Second, we compare the morphology. The problem is that the microhydrodynamic and the Doi-Ohta characterizations of the morphology are not directly comparable. Nevertheless, we still can compare the relaxation times. Palierne's microhydrodynamic analysis [25] gives a relaxation time for the droplet shape at low frequencies,

$$\tau_c = \frac{\eta_{\text{out}} r_0}{\Gamma}\frac{(19p + 16)(2p + 3)}{40(p + 1)}, \tag{49}$$

where r_0, is the initial radius of the droplet, $r_0 = 3\phi/Q_0$, and ϕ is the volume fraction of the dispersed phase. By equating (49) with (45) we obtain the second equation relating the microhydrodynamic material parameters and (37):

$$\frac{1}{Q_0}\frac{1}{(1/\mu - 1)d_1 + (2\kappa/27\mu_1)(4\beta_q + 3)} = r_0\frac{(19p + 16)(2p + 3)}{40(p + 1)}. \tag{50}$$

Now we proceed to draw consequences of Eqs. (48) and (50). We note that they are two nonlinear algebraic equations relating five unknowns (37). Among all possible solutions we look for those satisfying the following properties: (i) $\mu_1 > 0$ (in order to satisfy the requirements put on the dissipation potential), and (ii) $1/\mu_1$ and μ_2/μ_1 tend to zero as $p \to 1$ (the advection is expected to be passive if $\eta_{\text{in}} \sim \eta_{\text{out}}$).

From the requirement (ii) we get

$$d_1 = \frac{16\mu}{105(1 - \mu)\phi}, \tag{51}$$

$$\beta_q = \frac{3}{5\phi} - \frac{3}{4}. \tag{52}$$

With these values of d_1 and β_q we then obtain

$$\mu_1 = \frac{7\kappa(19p + 16)(2p + 3)}{3[175(p + 1) - 2(19p + 16)(2p + 3)]}, \tag{53}$$

$$\mu_2 = \frac{7[(19p + 16)(2p + 3) - 25(5p + 2)]}{3[175(p + 1) - 2(19p + 16)(2p + 3)]}. \tag{54}$$

We note that the requirement (i) is satisfied if $p < 1$. But this restriction is not a loss of generality since the Doi-Ohta characterization of the morphology does not distinguish between "inside" and "outside." In the comparison with experimental data we shall thus consider p to be always a ratio of the smaller viscosity coefficient to the larger viscosity coefficient. The difference between the experimental data of the blend with p and $1/p$ (see Sec. IV D) will be expressed in other parameters (in particular, in the parameter μ—arising already in the original Doi-Ohta theory—that is, at this point, left undetermined).

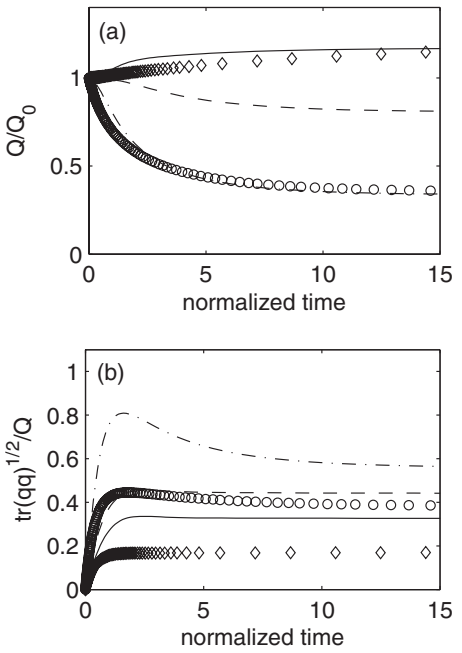

FIG. 1. Influence of μ on the time evolution of the area density Q/Q_0 (a) and on the deformation $[\mathrm{tr}(\boldsymbol{q}\cdot\boldsymbol{q})]^{1/2}/Q$ (b) of the interface of blends submitted to a start-up simple shear flow. (○) and (◇) correspond to the DO1 and DO2 models, respectively; the curves (—), (--), and (-.-) correspond to the active DO model with μ =0.2, 0.5, and 0.8, respectively.

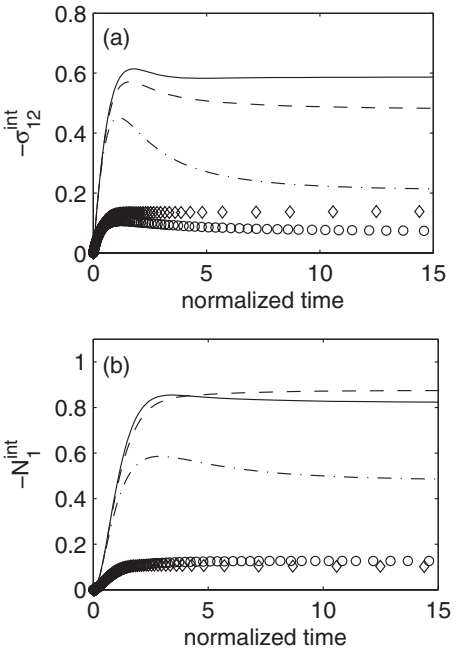

FIG. 2. Influences of μ on the time evolution of the normalized interfacial shear stress $\sigma_{12}^{\mathrm{int}}$ and the first normal stress difference N_1^{int} of blends submitted to a start-up simple shear flow. (○) and (◇) correspond to the DO1 and DO2 models, respectively; the curves (—), (--), and (-.-) correspond to the active DO model with μ =0.2, 0.5, and 0.8, respectively.

C. Effect of μ

In the original Doi-Ohta equations, the parameter μ describes the ratio of the relaxation rate of the area density (the size of the interface) to that of the deformation of the interface (the deformation of its shape). The range of μ is from 0 to 1. Although the physical meaning of the parameter μ remains the same in the present active advection model, its influence on the morphological and the rheological is different.

Figures 1 and 2 illustrate the influences of μ on the transient behavior of the immiscible blend. The applied flow field is a start-up simple shear flow, Q/Q_0 is the normalized area density, $\mathrm{tr}(\boldsymbol{q}\cdot\boldsymbol{q})^{1/2}/Q$ describes the normalized average deformation of the interface, and $\sigma_{12}^{\mathrm{int}}$ and N_1^{int} are the interface contributions to the normalized (i.e., divided by $\eta_{\mathrm{out}}\dot{\gamma}$) shear stress and the first normal stress difference. The calculations are made by choosing η_{out}=93 Pa s, p=0.5, ϕ =30%, $Q_0=5\times10^4$ m^{-1}, $\dot{\gamma}$=0.5 s^{-1}, and μ takes three different values: 0.2, 0.5, and 0.8. The results of the DO1 (symbol ○) and DO2 models (symbol ◇) are also displayed, with d_1 and μ taking the same values as the active DO model with μ=0.5 (dashed line). Figure 1 shows that when μ takes small values, for example, $\mu<0.2$ with the above initial conditions, the area density increases monotonically with time. This corresponds to the processes of deformation or breakup of droplets. Upon increasing μ ($\mu>0.5$ here), the interfacial area densities show monotonic decreases with time. This indicates that the coalescence of droplets takes place. The larger μ, the stronger is the effect of the coalescence. As a consequence of the decrease of the area density with larger μ, the average deformation of the interface increases because larger droplets with the same interfacial tension are easier to deform under the same external flow. The figure also displays a larger overshoot of the deformation for larger droplets with smaller area density. The present model is the DO2 model modified with active advection. The comparison of the dashed lines (active DO model with μ=0.5) and ◇ symbols (DO2 model with the same d_1 and μ) indicates that the DO2 model overestimates the area density and underestimates the global deformation of interfaces.

As to the rheological properties depicted in Fig. 2, it can be seen that both the shear stress and the first normal stress difference decrease as μ increases. This is in accordance with the decreased area density displayed in Fig. 1. Since smaller Q and $\boldsymbol{q}$ result in smaller stresses. Figure 2 also displays that the overshoots become more prominent as μ is enhanced because the size of the droplet is increased with lower area density. We can also see from these graphs that the DO2 model underestimates both the shear stress and the first stress differences. This is because the expression for the stress tensor used in the original Doi-Ohta model is incomplete. The contribution due to the deformation of the interface, i.e., the terms involving β_q in the last equation of (33), is missing in the original Doi-Ohta model.

The influence of μ on predicted steady-state values of morphological and rheological functions is displayed on Figs. 3 and 4. η^{int} and N_1^{int} are the interface contributions to the viscosity and the first normal stress difference. The calculations are made by choosing η_m=93 Pa s, p=0.5, ϕ =30%, $\Gamma=1\times10^{-3}$ N m, $Q_0=1\times10^4$ m^{-1}, and μ takes three different values: 0.2, 0.5, and 0.8. When the shear rate varies,

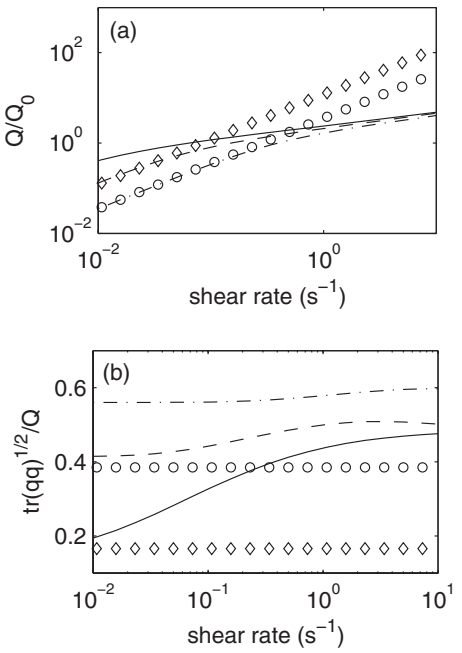

FIG. 3. Influence of μ on steady-state values of the normalized area density (a) and the deformation (b) of the interface of blends submitted to a simple shear flow. (○) and (◇) correspond to the DO1 and DO2 models, respectively; the curves (—), (--), and (-.-) correspond to the active DO model with μ=0.2, 0.5, and 0.8, respectively.

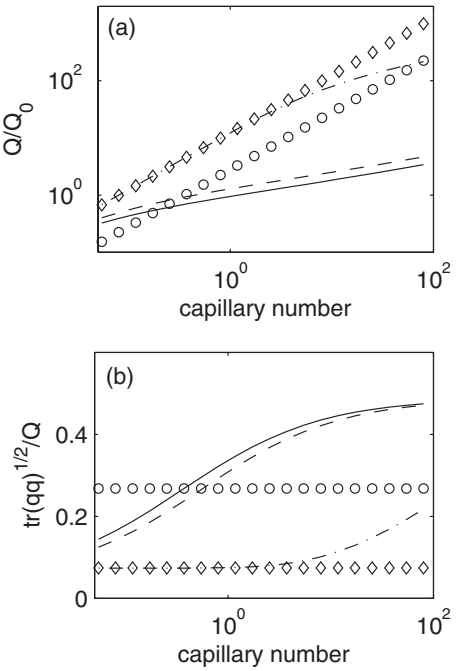

FIG. 5. Influences of p on steady-state values of the normalized area density (a) and the deformation (b) of the interface of blends presented as functions of $\mathcal{C}$. (○) and (◇) correspond to the DO1 and DO2 models, respectively; the curves (—), (--), and (-.-) correspond to the active DO model with p=0.1, 0.5, and $1-1\times10^{-5}$, respectively.

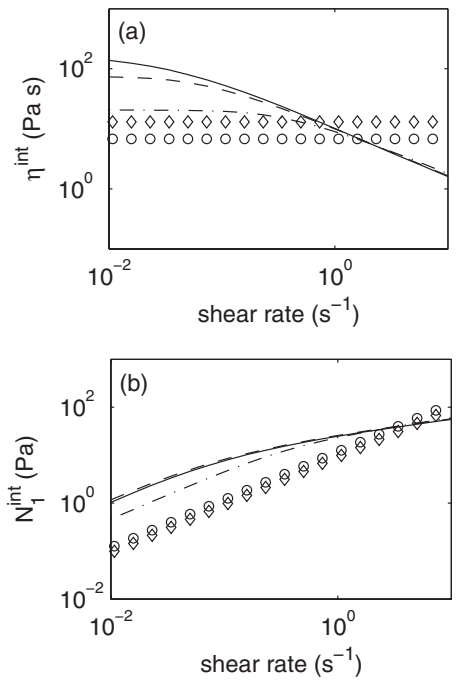

FIG. 4. Influence of μ on steady-state values of the normalized interfacial shear stress σ_{12}^{int} and the first normal stress difference N_1^{int} presented as functions of the shear rate. (○) and (◇) correspond to the DO1 and DO2 models, respectively; the curves (—), (--), and (-.-) correspond to the active DO model with μ=0.2, 0.5, and 0.8, respectively.

we observe in Fig. 3 that an increase in μ leads to a decrease in the area density and an increase in the deformation of the interface, just as the figure of the transient states shows. Moreover, we note that the influence of μ is more pronounced at smaller shear rates, and become less pronounced as the shear rate increases. Figure 3 also indicates that both the DO1 model and the DO2 model predict a linear relation between Q/Q_0 and $\dot{\gamma}$. These relations become nonlinear in the active DO model. Another difference between the DO1 and DO2 models on one side and the active DO model model on the other side is in the dependence of the steady-state value of the interface deformation on the shear rate. Both DO1 and DO2 models predict no dependence but the active DO model predicts an increase with an increase of the shear rate.

The rheological properties at steady states are displayed in Fig. 4. We see that an increase of μ causes both the shear stress and first normal stress difference to decrease. This effect becomes less pronounced in the region of higher shear rates. The active DO model predicts a shear thinning behavior, while the viscosities predicted by the two Doi-Ohta models are constant over the different shear rates. From the expression of the stress tensor, we conclude that the shear thinning is mainly caused by (i) the decrease of the deformation part of the stress tensor (i.e., the terms involving β_q), and (ii) the active advection. The figure shows also that N_1 predicted by the active DO model becomes nonlinear as a function of shear rate. Moreover, we note that η and N_1 are insensitive to changes of μ at high shear rates.

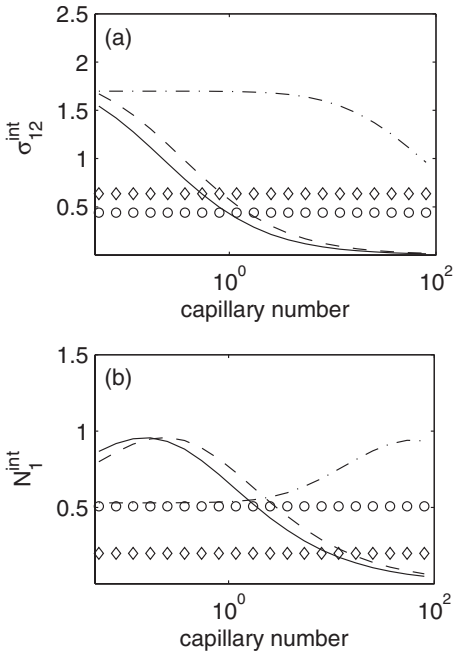

FIG. 6. Influence of p on steady-state values of the normalized interfacial shear stress σ_{12}^{int} and the first normal stress difference N_1^{int} presented as functions of $\mathcal{C}$. (○) and (◇) correspond to the DO1 and DO2 models, respectively; the curves (—), (--), and (-.-) correspond to the active DO model with $p=0.1$, 0.5, and $1-1\times10^{-5}$, respectively.

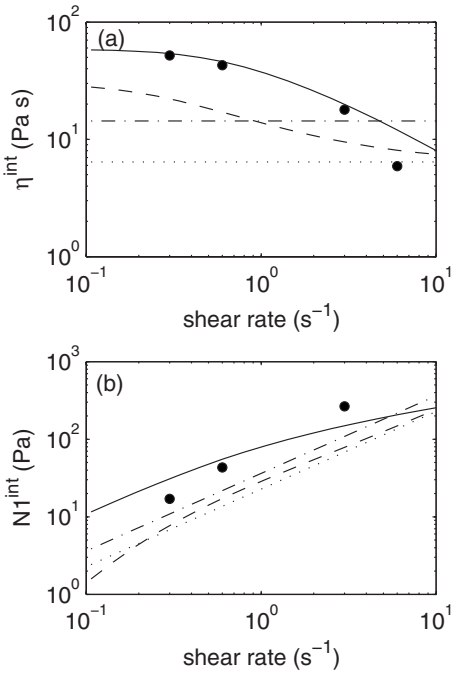

FIG. 7. Steady-state interfacial viscosity (a) and the first normal stress difference (b) for the DO1 model (···); for the DO2 model (-.-); for the WOE model (- - -); for the active DO model (—); by (●) we represent the Vinckier *et al.* [29] experimental data.

D. Effect of p and $\mathcal{C}$

The viscosity ratio p is defined as the ratio of the viscosity of the dispersed phase to that of the the matrix phase. It describes the nonuniformity of the material properties of the immiscible blends, and plays the most important role in controlling the extent of perturbation on the applied flow field. The original Doi-Ohta model considers only $p=1$, corresponding to passive advection, which is a special case of the active advection. The capillary number $\mathcal{C}$ is another parameter that affects the properties of emulsions. In the following paragraph, we will discuss the effect of p and $\mathcal{C}$ on rheological and morphological predictions of active DO model.

Figures 5 and 6 illustrate the influence of p and $\mathcal{C}$ on steady-state morphological and rheological behavior. σ_{12}^{int} and N_1^{int} are the interface contributions to the normalized (i.e., divided by $\eta_{out}\dot{\gamma}$) shear stress and the first normal stress difference. The calculations are made with $\phi=30\%$, $\kappa=9.514\times10^7$, $\mu=0.1$, and p takes three different values: 0.1, 0.5, and $1-1\times10^{-5}$. It can be seen from Fig. 5 that, if p takes a value very close to unity, the interface is convected in the active DO model just as in the DO2 model at small capillary numbers. This implies that passive advection takes place for $p=1$. When p deviates from unity, the predicted area density is less than that of the DO2 model, which indicates a nonaffine advection. However, the global deformation $\mathrm{tr}(\boldsymbol{q}\cdot\boldsymbol{q})^{1/2}/Q$ is increased because the decrease of Q is larger than the decrease of $\mathrm{tr}(\boldsymbol{q}\cdot\boldsymbol{q})^{1/2}$. This means that during the nonaffine advection the break up of the droplets in deformations is less frequent than during the affine advection.

We turn now to the interfacial shear stress represented in Fig. 6. We can see that the shear stress is largest for the passive advection with $p=1$. We also note that in the zero-shear-rate limit it reaches the value 1.75 which is in agreement with Taylor's theory. The first normal stress difference shows, for passive advection, an increase when $\mathcal{C}$ increases, but a decrease when $\mathcal{C}$ increases for nonaffine advection.

E. Comparison with experimental data and with other models

In this section we compare the results predicted by the active DO model with experimental data. In order to facili-

TABLE I. Parameters used to predict the rheological properties of the immiscible blend of PIB-PDMS (70%-30%) in the experiments of Vinckier *et al.*[29].

Model	p	η_{out} (Pa s)	ϕ	Γ(mN/m)	Q_0 (m^{-1})	d_1	μ
DO1		93	0.3	2.8	1.4×10^4	0.53	0.51
DO2		93	0.3	2.8	1.4×10^4	0.53	0.51
WOE		93	0.3	2.8	1.4×10^4	0.53	0.51
Active DO	1.075	93	0.3	2.8	1.4×10^4		0.51

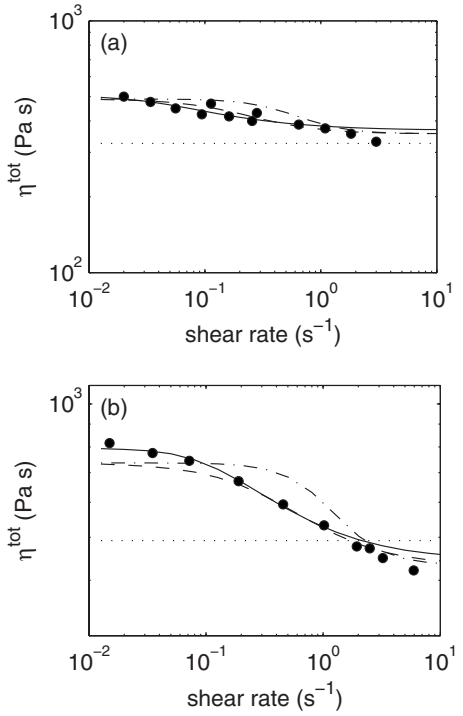

FIG. 8. Steady-state interfacial viscosity of (a) 30-70 and (b) 70-30 blends of PIB-PDMS. The curve (···) corresponds to the LP model; (-.-) to the FA model, (--) to the extended FA model and (—) to the active DO model; (●) represents the experimental data taken from Grizzuti *et al.* [23].

tate the illustration, we also present predictions of other models, including the DO1, DO2, WOE, LP, and FA models. The experimental data are taken from Vinckier *et al.* [29], Grizzuti *et al.* [23], and Lacroix *et al.* [12]. All the material data and initial conditions (if reported) are the same as those in the experiments. The phenomenological parameter, μ is determined by fitting the data.

First, we consider the steady-state rheological properties of semidilute emulsions. The experimental data are taken from Vinckier *et al.* [29] for the model system of poly(isobutene) (PIB) and poly(dimethylsiloxane) (PDMS) with 70% PIB as matrix. Both components show nearly constant viscosity and a slight elasticity for the shear rates in the interval from 0.3 to 6 s^{-1}. The interfacial tension is 2.8×10^{-3} N/m. Figure 7 shows the comparison of the contributions of the interface to the viscosity coefficient η^{int} and the first normal stress difference N_1^{int}. The experimental values are obtained by subtracting the bulk contribution by using the following linear mixing rule:

$$\eta^{tot} = \eta^{int} + \eta^{com},$$

$$N_1^{tot} = N_1^{int} + N_1^{com}, \tag{55}$$

where η^{com} and N_1^{com} are the volume-averaged values for both components. In addition to the two original Doi-Ohta models, DO1 and DO2, the predictions of the WOE model are also presented. Since the initial area density Q_0 was not provided in the experimental data, we take it as another fitting parameters here. The values of parameters used in the models are listed in Table I.

TABLE II. Parameters used to predict the rheological properties of the PIB-PDMS (30-70) blend in the experiments of Grizzuti *et al.*[23].

Model	p	η_{out} (Pa s)	ϕ	Γ (mN/m)	Q_0 (m^{-1})	ν	d_1	μ
LP		310	0.3	3	3×10^3	0.9	1.08	0.68
Active DO	1.61	310	0.3	3	3×10^3			0.68

We first compare the two original Doi-Ohta models. We can see that with the same values of the material parameters the DO2 model gives higher values for the viscosity coefficient and for the first normal stress difference. But both DO1 and DO2 models predict constant viscosity coefficients and thus fail to predict the experimentally observed shear thinning phenomena. The WOE model predicts qualitatively the right trend of the shear thinning, but the predictions are not quantitatively good enough. The predictions of the WOE model for the first normal stress difference also look worse than those of the original Doi-Ohta models. We note that the active DO model not only predicts the shear thinning behavior but it also gives the best quantitative fitting to the experimental data. The improvement in predictions of the active DO model is mainly a consequence of the more realistic consideration of the advection of the interface, and the more complete expression for the stress tensor.

Figure 8 displays other predictions of the active DO model and compares them with the experimental data, the LP model, and the FA model (the extended version of the FA model due to Grizzuti *et al.* [23]. The steady-state viscosity of the emulsion in the extended FA model is written as [23]

$$\eta = \frac{\eta_{out}}{1+\theta_1}\left[1 + \frac{5p+2}{2p+2}\phi + \theta_1\left(1 + \frac{5p+2}{2p+2}\phi - \frac{19p+16}{2(p+1)(2p+3)}\phi\right)\right], \tag{56}$$

where

$$\theta_1 = \left(\frac{(2p+3)(19p+16)}{40(p+1)}\frac{\eta_m K}{\Gamma}\dot{\gamma}^{(1-\theta_2)}\right)^2. \tag{57}$$

Here K and θ_2 are the parameters determined by linear viscoelastic measurements. Since the extended FA model gives good predictions for semiconcentrated emulsions, we are including it in the collection of models with which we are comparing the active DO model. The experimental data are taken from Grizzuti *et al.* [23] for an immiscible model polymer blend of PIB-PDMS system subjected to a simple shear flow. Figure 8(a) addresses the 30-70 system in 9 °C with the volume ratio of 30% of PIB as the droplet phase. Figure 8(b) is for the 70-30 system at 9 °C with the volume ratio of 70% of PIB as the matrix phase. The interfacial tension was reported to be 3×10^{-3}N/m. The linear mixing rule, Eq. (55), is used to calculate the total stress of the blends. The viscosities of both of its components are taken to be their

TABLE III. Parameters used to predict the rheological properties of the PIB-PDMS (70-30) blend in the experiments of Grizzuti *et al.* [23].

Model	p	η_{out} (Pa s)	ϕ	Γ (mN/m)	Q_0 (m^{-1})	ν	d_1	μ
LP		500	0.3	3	3×10^4	0.9	0.56	0.525
Active DO	0.62	500	0.3	3	3×10^4			0.525

zero-shear values, that is, $\eta_{PIB}=500$ Pa s and $\eta_{PDMS}=310$ Pa s. The values of the parameters used by the LP model and the active DO model are listed in Tables II and III. Since the initial radius Q_0 is not known in the experiments, we use both Q_0 and μ as fitting parameters. The critical steady-state droplet radii used in the FA model are taken as 6 μm for the 30-70 system and 3 μm for the 70-30 system, corresponding to the measured values at shear rate $\dot{\gamma}=3$ s^{-1}. The parameters K and θ_2 are those used by Grizzuti *et al.* [23]. As shown in Figs. 8(a) and 8(b), the LP model, just like the original DO models, fails to predict the shear thinning behavior. Introduction of more parameters does not change the steady-state viscosity dependence on the shear rate. The FA model (without adjustable parameters) can only qualitatively predict the shear thinning behavior. The extended FA model, with an added relation (based on results of measurements) between the droplet radius and the shear rates, can give very good results over the larger-shear-rate region.

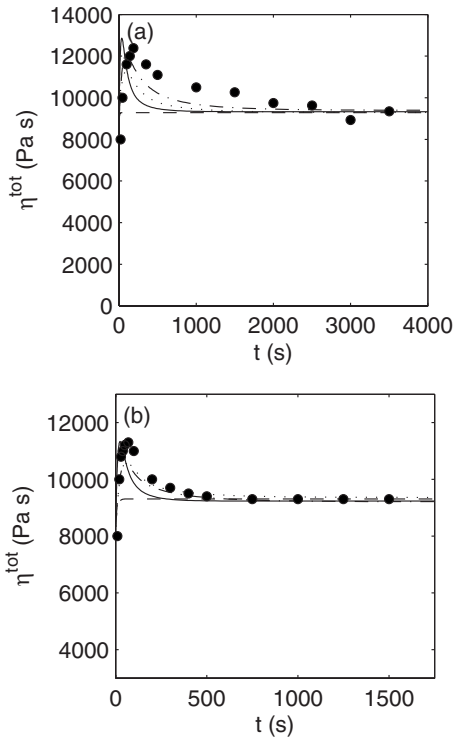

FIG. 9. Time evolution of the total viscosity under start-up simple shear flows with $\dot{\gamma}=0.0126$ (a) and (b) 0.0317 s^{-1}. The curves (···) correspond to the DO1 model, (-·-) to the DO2 model, (--) to the WOE model, (—) to the active DO model, and (●) represent experimental data taken from Lacroix *et al.* [12].

TABLE IV. Parameters used to predict the rheological properties of the PP-(EVA-EMA) blend in the experiments of Lacroix *et al.*[12] for $\dot{\gamma}=0.0126$ s^{-1}.

Model	p	η_m (Pa s)	ϕ	Γ (mN/m)	r_0 (μm)	d_1	μ
DO1		11650	0.285	1.2	3.75	0.6	0.65
DO2		11650	0.285	1.2	3.75	1	0.65
WOE		11650	0.285	1.2	3.75	4.5	0.62
Active DO	0.126	11650	0.285	1.2	3.75		0.95

However, both FA models underestimate the viscosity at low shear rates. The predictions of the active DO model are in good agreement with experimental data. It gives results that are better than the results for the extended FA model except at the region of large shear rates. The deviations of both models from the experimental data at high shear rates may be partially caused by the shear thinning of PDMS itself (experimental data of Grizzuti *et al.* [23] shows that the viscosity of pure PDMS has already dropped near $\dot{\gamma}=5$ s^{-1}).

In Fig. 9 we investigate the active DO model in start-up simple shear flows. The models with which we make the comparison are selected to be the DO1, DO2, and WOE models. The experimental data are taken from Lacroix *et al.* [12] for immiscible polymer blends of polypropylene/ethuylenevinylacetate-etylenemethylacrylate [PP-(EVA-EMA)] with the volume fraction 28.5% of EVA-EMA as the droplet phase. Although the components are non-Newtonian fluids, the dependence of the steady-state viscosities of the pure components on the shear rate is not important since we consider only the transient properties of the blends at a fixed shear rate. Results of the experimental observations indicate that the two components do not exhibit any measurable overshoot at start-up flows. Consequently, the overshoots observed in the graphs are totally due to the presence of the interface. Again, the linear mixing rule, Eq. (55), is used. The data that we select in Figs. 9(a) and 9(b) correspond to $\dot{\gamma}=0.0126$ and 0.0317 s^{-1}, respectively. The initial value of the surface area density is calculated as $Q_0=3\phi/r_0$, with ϕ representing the volume fraction of the droplet phase and r_0 being the measured initial volume-averaged droplet radius. The parameters used in the calculations are listed in Tables IV and V. We can see that the two original DO models can predict well the steady state but underestimate the overshoots observed in the experiments, while the active DO model can provide good predictions of both the steady-state values and

TABLE V. Parameters used to predict the rheological properties of the PP-(EVA-EMA) blend in the experiments of Lacroix *et al.*[12] for $\dot{\gamma}=0.0317$ s^{-1}.

Model	p	η_m (Pa s)	ϕ	Γ (mN/m)	r_0 (μm)	d_1	μ
DO1		11080	0.285	1.2	3.75	0.3	0.65
DO2		11080	0.285	1.2	3.75	0.7	0.65
WOE		11080	0.285	1.2	3.75	2.2	0.65
Active DO	0.131	11080	0.285	1.2	3.75		0.92

the height of the overshoot. However, the time taken for the blends to reach the maximum of the overshoot predicted by the active DO model is less than in the experimental observations. The WOE model, as shown in Fig. 9, fails to predict the overshoot. A possible explanation for this is that the modification introduced in the WOE model limits its applicability to, essentially, the absence of breakup and coalescence (which likely play an important role in the initial deformations in start-up flows). It is worthwhile to note that in the active DO model a larger μ is fitted for the data of $\dot{\gamma}=0.0126\ s^{-1}$ than for those of $\dot{\gamma}=0.0317\ s^{-1}$. This is in agreement with the experimental observations on the relationship between the average steady droplet size and shear rate, where the droplet size is proportional to the inverse of shear rate. Since a larger μ means a stronger tendency for droplets to coalescence, the smaller the shear rates the easier it is for droplets to collide and coalesce to form larger droplets.

To sum up, it is evident that the active DO model, although using one tewer free parameter, can give the best predictions among all the Doi-Ohta-type models.

V. CONCLUDING REMARKS

The most frequently used point of departure for discussing immiscible blends is microhydrodynamics [30]. The physics entering the governing equations consists of the rheological properties of the two fluids, mechanical properties of the interface, and the interface-bulk fluid interactions. All the material parameters involved can be, at least in principle, obtained in independent microhydrodynamic measurements. The governing equations are easily written but they are difficult to solve. Moreover, their solutions provide only the morphology. The transformation *morphology* $\rightarrow$*rheology* requires additional physical input and approximations.

In this paper we take a different (a mesoscopic) path. We regard the immiscible blend as a single fluid involving an internal structure. How do we characterize the internal structure? We follow Doi and Ohta [1] and us the surface area per unit volume (Q) and the anisotropy tensor ($\boldsymbol{q}$). The new physics (relative to [1]) that we are bringing is the perturbation of the overall flow due to the presence of the interface and the "rheological inhomogeneity" of the two fluids. In order to be able to express the new physics we adopt an additional state variable (a tensor $\boldsymbol{w}$ that is a conjugate of the perturbed velocity gradient). We are taking the mesoscopic viewpoint for two reasons. First, we want to search for new physics emerging in the overall (mesoscopic) hydrodynamics of immiscible blends. Such a search is, on the microhydrodynamic path, entangled hopelessly with the enormous difficulty of solving the microhydrodynamic governing equations. Second, we want to satisfy the practical need of providing a relatively simple formulation that can be used in, say, calculations involved in polymer processing operations.

The disadvantage of the mesoscopic approach taken in this paper is that the material parameters quantifying the physics involved (mesoscopic material parameters) can be only partially determined by the comparison with microhydrodynamic theories. The remaining parameters (arising already in the original Doi-Ohta theory) have to be obtained from measurements belonging to the same mesoscopic level (as, for instance, the material parameters of classical hydrodynamics are usually obtained from hydrodynamic measurements and not from microscopic measurements of atoms composing the fluid under consideration).

The advantage of the Doi-Ohta approach is the simplicity and transparency of the governing equations. We construct them by filling the general framework called GENERIC. The framework itself guarantees the agreement of solutions with experimental observations constituting the basis of mechanics and thermodynamics. The framework is filled by insight into the physics taking place in the flowing immiscible blend. We call the process of filling the GENERIC framework a "GENERIC constitutive relation." We use this terminology in order to make a direct analogy with the familiar term "constitutive relations" used for the process of filling another abstract framework, namely, the framework of local conservation laws (balance equations, the time derivative of a field equals the divergence of a flux), constituting the basis of classical hydrodynamics. If the fluids under consideration have an internal structure whose time evolution takes place on a time scale comparable with the time scale on which the hydrodynamic fields evolve the the abstract framework of local conservations laws is insufficient and has to be replaced by the framework of GENERIC.

The final output of the model that can be compared with experimental data is the following: (i) information about the morphology of the interface (namely, the information expressed in the orientation tensor $\boldsymbol{q}$ and the density of the surface area of the interface Q), and (ii) the rheological behavior. In this paper we concentrate on predictions of nonlinear rheological responses to imposed shear flows and their comparison with predictions of the original Doi-Ohta model and experimental data reported in the literature. In the original Doi-Ohta model we distinguish four versions, the Doi-Ohta 1, Doi-Ohta 2, Lee-Park, and Wagner-Ottinger-Edwards models, corresponding to four variations in the selection of phenomenological quantities entering the model. In general, we find that the more faithful to reality (i.e., closer to microhydrodynamics) consideration of the physics in the active Doi-Ohta model improves the agreement of predictions with the observed behavior.

ACKNOWLEDGMENT

This research has been partially supported by the Natural Sciences and Engineering Research Council of Canada.

[1] M. Doi and T. Ohta, J. Chem. Phys. **95**, 1242 (1991).
[2] J. F. Gu and M. Grmela, J. Non-Newtonian Fluid Mech. **152**, 12 (2008).
[3] M. Grmela, Contemp. Math. **28**, 125 (1984).
[4] M. Grmela, Physica D **21**, 179 (1986).
[5] M. Grmela, *Mesoscopic Dynamic and Thermodynamic: Application to Polymer Fluids*. Lecture Notes in Physics Vol. 381, (Springer, Berlin, 1991) p. 99.
[6] A. N. Beris and B. J. Edwards, *Thermodynamics of Flowing Systems* 1st ed. (Oxford University Press, New York, 1994).
[7] M. Grmela and H. C. Ottinger, Phys. Rev. E **56**, 6620 (1997).
[8] H. C. Ottinger and M. Grmela, Phys. Rev. E **56**, 6633 (1997).
[9] M. Grmela, Physica A **309**, 304 (2002).
[10] H. C. Ottinger, *Beyond Equilibrium Thermodynamics* (Wiley, New York, 2005).
[11] M. Grmela and A. Ait-Kadi, J. Non-Newtonian Fluid Mech. **55**, 191 (1994).
[12] C. Lacroix, M. Grmela, and P. J. Carreau, J. Rheol. **42**, 41 (1998).
[13] A. Clebsch, J. Reine Angew. Math. **56**, 1 (1895).
[14] V. I. Arnold, Ann. Inst. Fourier **16**, 319 (1966).
[15] J. E. Marsden and A. Weinstein, Physica D **7**, 305 (1983).
[16] J. F. Gu, M. Grmela, and M. Bousmina, Phys. Fluids **20**, 043102 (2008).
[17] V. G. Baidakov, G. Sh. Boltachev, and G. G. Chernykh, Phys. Rev. E **70**, 011603 (2004).
[18] W. Helfrich, Z. Naturforsch. C **29**, 510 (1974).
[19] J. Pellicer, J. A. Manzanares, and S. Mafe, Am. J. Phys. **63**, 542 (1995).
[20] H. M. Lee and O. O. Park, J. Rheol. **38**, 1405 (1994).
[21] J. Wagner, H. C. Ottinger, and B. J. Edwards, AIChE J. **45**, 1169 (1999).
[22] N. A. Frankel, and A. Acrivos, J. Fluid Mech. **44**, 65 (1970).
[23] N. Grizzuti, G. Buonocore, and G. Iorio, J. Rheol. **44**, 149 (2000).
[24] G. I. Taylor, Proc. R. Soc. London, Ser. A **138**, 41 (1932).
[25] J. F. Palierne, J. Rheol. **29**, 204 (1990); **30**, 497 (1991).
[26] Y. Takahashi, N. Kurashima, I. Noda, and M. Doi, J. Rheol. **38**, 699 (1994).
[27] G. K. Guenther and D. G. Baird, J. Rheol. **40**, 1 (1996).
[28] I. Vinckier and H. M. Laun, J. Rheol. **45**, 1373 (2001).
[29] I. Vinckier, M. Minale, J. Mewis, P. Moldenaers, Colloids Surf., A **150**, 217 (1999).
[30] S. Kim and S. J. Karilla, *Microhydrodynamics* (Butterworth-Heinemann, London, (1991).